TU/e EINDHOVEN UNIVERSITY OF TECHNOLOGY

3D bioprinting of complex channels : effects of material, orientation, geometry, and cell embedding

Citation for published version (APA):
Wüst, S., Müller, R., & Hofmann, S. (2015). 3D bioprinting of complex channels : effects of material, orientation, geometry, and cell embedding. *Journal of Biomedical Materials Research, Part A*, *103*(8), 2558-2570. https://doi.org/10.1002/jbm.a.35393

DOI:
10.1002/jbm.a.35393

Document status and date:
Published: 01/01/2015

Document Version:
Publisher's PDF, also known as Version of Record (includes final page, issue and volume numbers)

Please check the document version of this publication:

• A submitted manuscript is the version of the article upon submission and before peer-review. There can be important differences between the submitted version and the official published version of record. People interested in the research are advised to contact the author for the final version of the publication, or visit the DOI to the publisher's website.
• The final author version and the galley proof are versions of the publication after peer review.
• The final published version features the final layout of the paper including the volume, issue and page numbers.

Link to publication

General rights
Copyright and moral rights for the publications made accessible in the public portal are retained by the authors and/or other copyright owners and it is a condition of accessing publications that users recognise and abide by the legal requirements associated with these rights.

• Users may download and print one copy of any publication from the public portal for the purpose of private study or research.
• You may not further distribute the material or use it for any profit-making activity or commercial gain
• You may freely distribute the URL identifying the publication in the public portal.

If the publication is distributed under the terms of Article 25fa of the Dutch Copyright Act, indicated by the "Taverne" license above, please follow below link for the End User Agreement:

www.tue.nl/taverne

Take down policy
If you believe that this document breaches copyright please contact us at:

openaccess@tue.nl

providing details and we will investigate your claim.

Download date: 16. Apr. 2021

Society For Biomaterials

3D Bioprinting of complex channels—Effects of material, orientation, geometry, and cell embedding

Silke Wüst,[1] Ralph Müller,[1] Sandra Hofmann[1,2,3]*

[1]Department of Health Sciences and Technology, Institute for Biomechanics, ETH Zurich, Zurich, 8093, Switzerland
[2]Department of Biomedical Engineering, Eindhoven University of Technology, P.O. Box 513, Eindhoven, MB 5600, The Netherlands
[3]Department of Biomedical Engineering, Institute for Complex Molecular Systems, Eindhoven University of Technology, P.O. Box 513, Eindhoven, MB 5600, The Netherlands

Received 28 August 2014; revised 19 November 2014; accepted 11 December 2014
Published online 00 Month 2014 in Wiley Online Library (wileyonlinelibrary.com). DOI: 10.1002/jbmm.a.35393

Abstract: Creating filled or hollow channels within 3D tissues has become increasingly important in tissue engineering. Channels can serve as vasculature enhancing medium perfusion or as conduits for nerve regeneration. The 3D biofabrication seems to be a promising method to generate these structures within 3D constructs layer-by-layer. In this study, geometry and interface of bioprinted channels were investigated with micro-computed tomography and fluorescent imaging. In filament printing, size and shape of printed channels are influenced by their orientation, which was analyzed by printing horizontally and vertically aligned channels, and by the ink, which was evaluated by comparing channels printed with an alginate-gelatin hydrogel or with an emulsion. The influence of geometry and cell-embedding in the hydrogel on feature size and shape was investigated by printing more complex channels. The generation of hollow channels, induced through leaching of a support phase, was monitored over time. Horizontally aligned channels provided 16× smaller cross-sectional areas than channels in vertical orientation. The smallest feature size of hydrogel filaments was twice as large compared to emulsion filaments. Feature size and shape depended on the geometry but did not alter when living cells were embedded. With that knowledge, channels can be consciously tailored to the particular needs. © 2014 Wiley Periodicals, Inc. J Biomed Mater Res Part A: 00A:000–000, 2014.

Key Words: filament-based 3D bioprinting, complex channels, structure orientation, hydrogel, cell-embedding

How to cite this article: Wüst S, Müller R, Hofmann S. 2014. 3D Bioprinting of complex channels—Effects of material, orientation, geometry, and cell embedding. J Biomed Mater Res Part A 2014:00A:000–000.

INTRODUCTION

One major challenge in tissue engineering nowadays is the lack of suitable techniques to generate artificial tissues containing a stable channel system. Because most tissues and all organs are vascularized, hollow channels are needed for the creation of vascular systems within engineered 3D tissues to guarantee homogeneous access to nutrients and oxygen, particularly for tissues of clinically relevant sizes.[1] Conventional methods to generate hollow channels include punching out a cylinder after the fabrication of a construct[2] or pouring a hydrogel in a mold which contains a fixed component in shape of the desired channel structure which can be leached afterwards.[3] However, these approaches are restricted to straight channels, which does not allow the generation of complex channel structures, or by an outer geometry limited to the shape of the mold.

Nerve regeneration is important to address, for example, paraplegia or quadriplegia induced by a spinal cord injury, as it is known that grafted neurons allow the formation of new circuits or the regeneration of injured axons.[4] Stable channels filled with a stimulative environment for neural cells can be used to guide newly forming nerves in direction and length.[5] So far, nerve regeneration has been approached with 2D patterns[6] or prefabricated hollow channels subsequently filled with hydrogel to stimulate neurons,[7] which is either limited to 2D or deals with the same limitations for the conventional fabrication of channels.

Biofabrication is a powerful tool to create artificial tissues by placing different materials and/or cells next to each other in predefined patterns.[8–10] With appropriate deposition techniques and processing conditions avoiding extreme temperatures, pH values, high shear stresses, and cytotoxic crosslinking processes, it was shown that biological material such as growth factors or cells can be included in the printing process with acceptable bioactivity preservation or survival rates. Filament-based deposition is usually the method of choice for printing cells concomitantly with the biomaterial due to its gentle processing conditions compared to

Correspondence to: S. Hofmann; e-mail: sahofmann@ethz.ch
Contract grant sponsor: RMS Foundation (Bettlach, Switzerland)

© 2014 WILEY PERIODICALS, INC.

droplet-based inkjet printing, where cells are exposed to high shear forces due to the small orifices. Constructs fabricated according to the desired pattern provide a basis for further tissue engineering with cellular self-assembly.[11]

Another critical aspect for 3D bioprinting is the selection of a suitable ink.[12] The biomaterial has to support cell attachment and maintain cellular functionality for proliferation and/or differentiation and maturation of the required tissue. Specific rheological and mechanical properties of the biomaterial are needed to provide both printability and mechanical stability to maintain construct integrity right after printing and during culture. The biomaterial used in this study is an alginate-gelatin hydrogel composite, due to its cell-friendly properties and the manifold potential applications ranging from tissue engineering various tissues to drug delivery a promising material for 3D bioprinting.[13–15] Alginate-gelatin was for example successfully used for liver tissue engineering[13] and to culture smooth muscle cells and aortic valve cells *in vitro*.[14] It can be enhanced with osteoinductive[16] and radiopaque[17] hydroxyapatite to increase cell attachment,[18] for applications in bone tissue engineering[18] or as contrast agent for μCT analysis.[15] By printing alginate-gelatin onto a cooled surface, gelatin acts as immediate stabilizer and individual printed filaments keep their initial shape.[15] Once the whole construct is printed alginate is chemically crosslinked with calcium ions for long-term stability[19] and to connect the individual filaments permanently.[15] Then the construct can be warmed up—gelatin probably dissolves, which has no impact on the stability, as the stability of the construct for cell culture at 37 °C is provided by alginate. Cell compatibility of the alginate-gelatin (hydroxyapatite) hydrogel composite used herein was investigated in a previous study and showed no reduction in the viability of embedded cells 3 days after printing.[15]

The 3D bioprinters are mostly advertised based on optimal conditions for performance, printing resolution and range of processable inks. The highest printing resolution can be achieved only with very few materials providing excellent rheological properties, which are most often not the cell-compatible biomaterials indicated as processable inks.

The aim of 3D biofabrication is to enable the generation of artificial tissues containing more complex structures. Early results in printing either filled or hollow channels were achieved,[20–25] affirming the use of bioprinting to create channels. Channels filled with material and cells were printed within permanent bulk material, and cells inside the channels proliferated while retaining their functionality,[20] formed confluent linings[21] or produced extracellular matrix.[22] Bioprinting of hollow channels within cell-free as well as cell-containing hydrogel bulk was realized with the bulk phase crosslinked, and the channel phase, consisting of a support material, leached after printing.[23,24] On commonality of all of these studies is that the channels were only printed in one orientation and the channel shape was mostly a cylinder. However, to create channel structures in larger tissues, branched systems that are organized in 3D over several printing planes are needed, and thus a combination of horizontally and vertically oriented structures will be a great enhancement. To be able to generate complex channel systems a systematic analysis of the individual components and influences of each parameter is necessary.

This study presents the systematic investigation of parameters influencing feature size and shape of 3D filament-printed channels within a 3D construct. In particular, the analyzed parameters are structure orientation, the used ink, geometry of the structure and the influence of embedded cells. The aim was to achieve the smallest possible feature size for each orientation and ink. This study shows for the first time to what extent structure orientation, ink, geometry and cell-embedding can influence feature size through a systematic analysis of the parameters. With this knowledge, more intricate artificial tissues containing complex channel systems can be designed and fabricated with filament-based deposition.

MATERIALS AND METHODS

Preparation of the inks

Low viscosity alginate provided as alginic acid derived from brown algae macrocystis pyrifera (Sigma–Aldrich, Buchs, Switzerland) was slowly mixed into phosphate buffered saline (PBS) (Medicago, Uppsala, Sweden) to a final concentration of 4% (w/v) and further stirred during 2 h. Gelatin type A from porcine skin (Sigma–Aldrich, Buchs, Switzerland) was dissolved in PBS in a concentration of 20% (w/v) and kept for 2 h at 60 °C to homogenize and dissolve remaining air bubbles. The alginate-PBS solution was thoroughly mixed with the gelatin-PBS solution in a 1:1 ratio, leading to a final concentration of 2% (w/v) alginate and 10% (w/v) gelatin. If needed, the hydrogel precursor was additionally enhanced with pure hydroxyapatite powder (Acros Organics, Geel, Belgium) in a concentration of 8% (w/v). To do so, hydroxyapatite was suspended at 16% (w/v) into PBS before the addition of alginate, and subsequently proceeded as described above. Hydrogel precursors for all experiments were pasteurized at 72 °C for 1 h and subsequently cooled to 8 °C before starting the experiments.

Nivea creme (Beiersdorf AG, Hamburg, Germany), a lipophilic water-in-oil emulsion, was used as control group. To render the emulsion radio-opaque for μCT imaging, the emulsion was enhanced with 8% (w/v) hydroxyapatite.

For the generation of hollow channels, gelatin served as support material. It was dissolved in PBS at 10% (w/v) and kept 2 h at 60 °C to homogenize with a subsequent pasteurization at 72 °C for 1 h.

3D bioprinting system

An open-source 2-syringe Fab@Home printer Model 2 (The Nextfab Store, Albuquerque, NM) modified with a heatable print-head, fabricated in-house was used as described previously.[15] All samples were printed by extruding filaments through a 27 gauge plastic dispense tip (EFD Nordson, Vilters, Switzerland), which corresponds to an inner tip diameter of 200 μm, onto a glass substrate. For hydrogel printing the material was warmed up to 40 °C, loaded into syringes and mounted on the print-head which was kept at 40 °C. The glass substrate surface was cooled to ∼10 °C, which

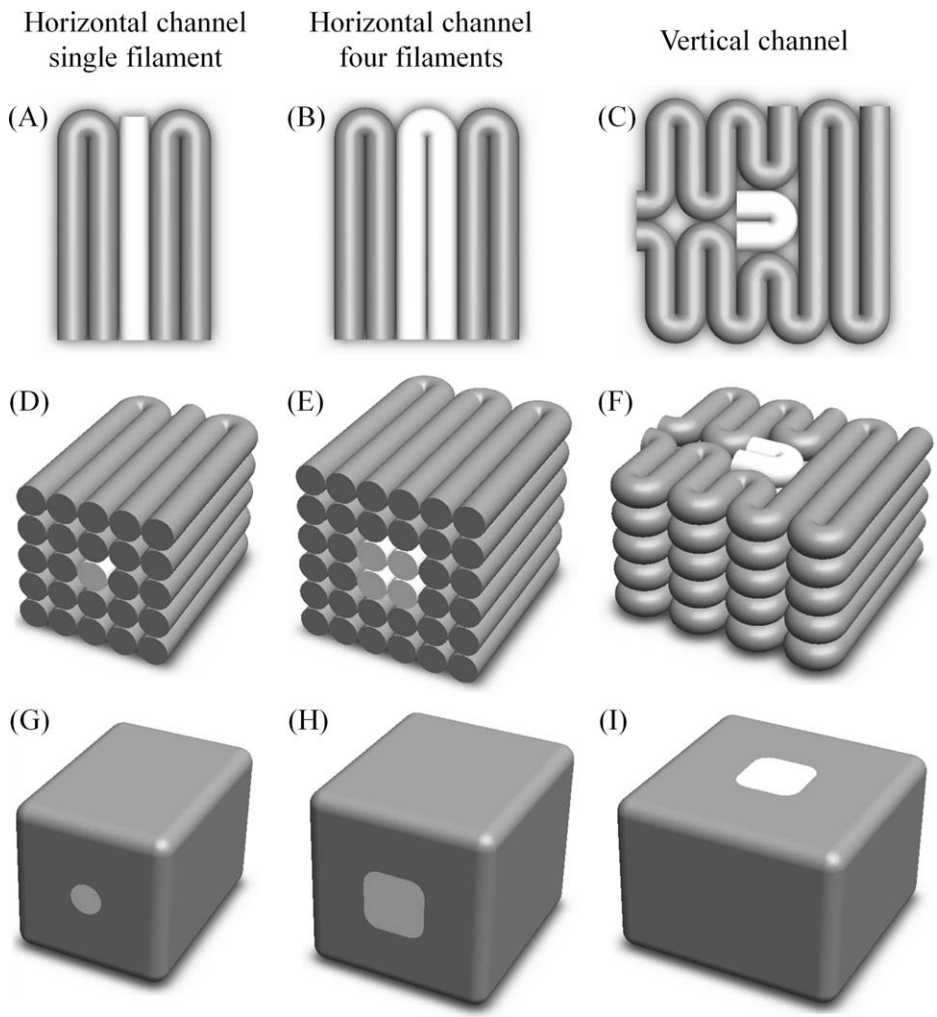

FIGURE 1. Schematic representation of the three different channels in bulk material: (A,D,G): horizontal channel consisting of a single filament; (B,E,H): horizontal channel consisting of four filaments and (C,F,I): vertical channel. (A–C) show the third layer of the printed construct indicating the printing path of both phases; (D–F) show the 3D objects indicating the printing path and amount printing layers per object and (G–I) show the 3D object with the channel as second phase.

led to immediate thermal solidification of the printed material. After printing, the hydrogel constructs were crosslinked in 2% (w/v) $CaCl_2$ (VWR, Dietikon, Switzerland) in PBS for 10 min. For printing the emulsion, the material was loaded into syringes and printed at room temperature directly onto the substrate; no crosslinking step was needed to provide structural stability.

Printing channels in horizontal and vertical orientation

To investigate the influence of channel orientation on feature size and shape of the cross-sectional areas, horizontally oriented channels were printed and compared to vertically oriented printed channels. Three different channels were analyzed: (i) a horizontal straight channel consisting of a single filament, (ii) a horizontal straight channel consisting of four filaments, and (iii) a vertical straight channel. Figure 1 shows a schematic representation of the various investigated channels, split into top view of the middle printed layer to show the channel phase [Fig. 1(A–C)], transversal view of the whole construct illustrating printing paths and amount of printing layers per object [Fig. 1(D–F)] and transversal view of the final object-to-be-printed [Fig. 1(G–I)]. Schematic images were created in SolidWorks 2011 (Waltham, MA). To visualize the channels inside the bulk, the bulk material of all constructs was enhanced with hydroxyapatite before printing to generate phase contrast for μCT imaging.

The common printing parameter, including printing speed, deposition rate, distance between adjacent filaments and layer height, were adapted for each ink-printer combination. The principles as used in this study to define ideal path width, which is the distance between adjacent filaments, and layer height are illustrated in Ref. 26. The printing path of both phases was optimized to achieve the smallest possible channel in each orientation. For the hydrogel precursor printing path speed was set to 2 mm s^{-1}, deposition rate was 0.0008 mm mm^{-1} (mm piston motion/mm travel) and a layer height of 350 μm was used. Path width was 500 μm for horizontal channels and 1 mm for vertical channels. The emulsion was printed with a path speed of 4 mm s^{-1} and a

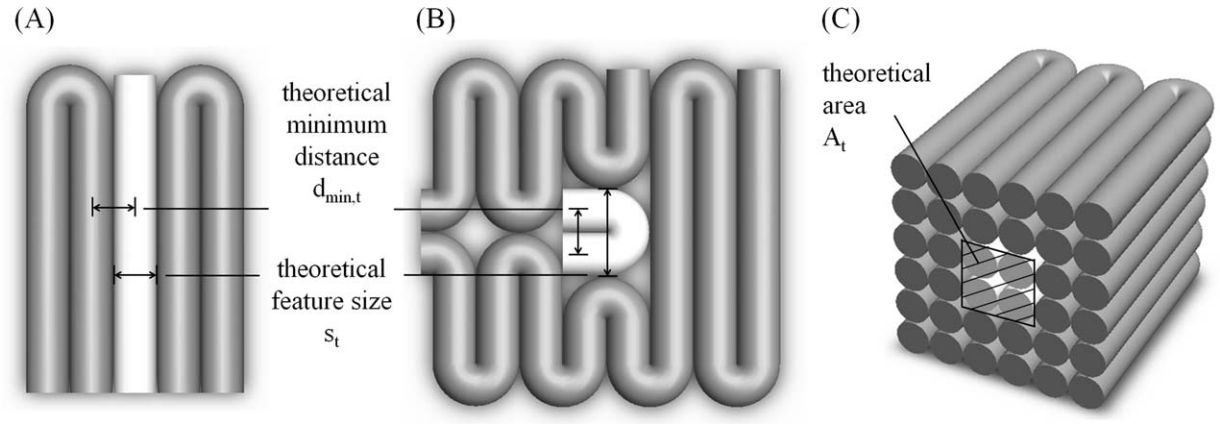

FIGURE 2. Parameters for geometrical analysis. Theoretical minimum distance $d_{min,t}$ indicates the smallest printable distance between two adjacent strands and theoretical feature size s_t indicates the width of the smallest possible feature size of the channel cross-section. Theoretical area A_t from channel cross-section is calculated from theoretical feature size with the assumption that printed strands fill the rectangle between adjacent strands and adjacent layers below and above.

deposition rate of 0.002 mm mm^{-1}. Layer height was 250 μm and the path width was 250 μm for horizontal channels and 500 μm for vertical channels.

μCT evaluation

Hydrogel samples were fixed in 10% neutral buffered formalin (Sigma–Aldrich, Buchs, Switzerland) for 24 h at room temperature immediately after crosslinking. Samples were washed in PBS and mounted in a μCT vial filled with PBS to avoid drying and the associated shrinkage of the hydrogel. Emulsion samples were mounted on their printing substrate into the μCT vial for imaging. The emulsion could not be fixed with buffered formalin due to its lipophilic character and was handled with great caution due to its weak stability.

Imaging was performed on a μCT 40 scanner (Scanco Medical AG, Brüttisellen, Switzerland). Isotropic nominal resolution was 16 μm, energy of the X-ray tube was set to 45 kVp and the intensity was 177 μA. Integration time was 300 ms and a frame averaging of 2 was used. The resulting images were processed with a constrained Gaussian filter with a filter width of 0.8 and a filter support of 1. Hydrogel samples measured in PBS were segmented with a threshold of 58 mg HA ccm^{-1} and the emulsion samples measured in air were segmented with a threshold of 21 mg HA ccm^{-1}, which were visually identified as best thresholds to separate the two phases. Morphometric analysis was performed based on parameters used for human bone biopsy analysis to assess bone volume, respectively channel volume in this study, within a defined volume of interest (VOI).[27,28]

Analysis of channel cross-sections

Cross-sectional areas of theoretical channels were calculated based on the printing parameters path width and layer height. Cross-sectional area of printed samples was evaluated by μCT image analysis. Parameters used to describe the various channels in horizontal and vertical orientation are illustrated in Figure 2. Theoretical minimum distance $d_{min,t}$ indicates the smallest possible printable distance between two adjacent filaments and theoretical feature size s_t describes the width respectively height of the smallest possible feature size of the channel cross-section. The cross-sections of horizontal channels lie in the xz plane which leads to an area derived from $s_{t,x}$ and $s_{t,z}$; cross-sections of vertical channels lie in the xy plane leading to an area derived from $s_{t,x}$ and $s_{t,y}$, respectively.

Theoretical area A_t was calculated from the minimal theoretical feature size in the two directions of the cross-section with the assumption that printed filaments fill the rectangle between adjacent filaments and adjacent layers below and above:

$$\boldsymbol{A}_t = \boldsymbol{s}_{t,1} \times \boldsymbol{s}_{t,2} \tag{1}$$

Printed channel volume V_p, was obtained evaluating μCT data with morphometric analysis.[28] Area of the printed samples A_p was calculated dividing V_p over the length l of the channel:

$$\boldsymbol{A}_p = \boldsymbol{V}_p \div \boldsymbol{l} \tag{2}$$

For hydrogel samples V_p over a length of $l = 5.6$ mm was used for horizontal channels and $l = 1.76$ mm for vertical channels; for emulsion samples $l = 4.8$ mm was used for horizontal channels consisting of a single filament, $l = 5.6$ mm for horizontal channels consisting of four filaments and $l = 0.48$ mm for vertical channels. The lengths were determined visually according to the longest possible intact channel volumes of $n = 5$ samples depending on the respective setup. Theoretical areas of the different channels were compared to areas calculated from the printed and imaged channels.

Printing more complex channels

A total of five structures with different channel geometries were generated to investigate the influence of the geometry on the smallest possible feature size and shape of the channel. The selected geometries represented channels in the shapes of L, T, S, U, and X, respectively, and contained

straight segments, different rectangular elements and intersections with connecting channels. The hydrogel constructs consisted all of five layers, the channels were oriented horizontally and located in the third printing layer. The printing scripts were individually written and the distance between adjacent filaments was adapted between 500 μm and 1 mm according to the pathway with respect to the curvatures within the geometry. Hydrogel compositions, printing parameter, the printing process, crosslinking and imaging were the same as for printing straight hydrogel channels (Preparation of the inks, 3D bioprinting system, and Printing channels in horizontal and vertical orientation sections). Image processing was performed with a filter width of 8 and a filter support of 8 for the Gaussian filter and samples were segmented with a threshold of 56 mg HA ccm^{-1}. Volume of the printed channels was analyzed as in μCT evaluation section and compared to the theoretical channel volume calculated from the channel length multiplied with A_t (Analysis of channel cross-sections section) within the same volume of interest. The evaluated VOI for all channel structures was $6.5 \times 5.5 \times 1.75$ mm^3.

Influence of cell-embedding on feature size and shape

For the printing of cell-containing constructs with more complex channels, alginate-gelatin hydrogel precursor was enhanced with cells in both phases. To provide aseptic conditions for the experiment, the printer was cleaned with 70% ethanol and moved into a biological safety cabinet (NU-440–600, NuAire, Plymouth, MN). Human mesenchymal stem cells (hMSCs) in sixth passage (P6) with the properties described in Ref. 29 were labeled with CellTracker™ Green CMFDA for the bulk phase and with CellTracker™ Red CMTPX for the channel phase (both CellTracker™ from Life Technologies, Ltd, Zug, Switzerland). For the labeling solution, both CellTracker™ were dissolved in anhydrous dimethylsulfoxide (DMSO) (Fluka-Chemie AG, Buchs, Switzerland), respectively at a concentration of 10 m*M* and subsequently mixed with Dulbecco's modified Eagle's medium (DMEM) (Invitrogen Basel, Switzerland) to achieve working solutions of 25 μ*M*. Per 10 million cells 500 μL of 25 μ*M* working solution was used. Cells were incubated in the CellTracker™ working solutions for 30 min followed by an incubation in control media consisting of DMEM with 10% fetal bovine serum (FBS), and 1% antibiotic/antimycotic solution (all obtained from Invitrogen, Basel, Switzerland) for another 30 min. Labeled cells were thoroughly mixed into 40 °C-tempered hydrogel precursors at a concentration of 10 million cells/mL precursor with a spatula. Each labeled solution was filled in one of the two syringes and mounted in the print-head. The same structures as in Printing more complex channels section were printed and crosslinked as described in 3D bioprinting system section. Control medium was additionally supplemented with 0.25% (w/v) $CaCl_2$ to maintain the structural integrity of the constructs during over-night incubation.

To assess the influence of cell-embedding on feature size and shape, the same geometries were printed with hydrogel alone. For this control group, the alginate-gelatin hydrogel precursor was labeled with fluorescein 5(6)-isothiocyanate (FITC) in the bulk phase and the hydrogel precursor for the channel phase was labeled with tetramethylrhodamine isothiocyanate (TRITC) (both from Sigma Aldrich, Buchs, Switzerland). FITC as well as TRITC were dissolved in anhydrous DMSO at a concentration of 5 mg mL^{-1} by mixing the solutions for 1 h on a plate-shaker protected from light. To stain alginate-gelatin with FITC, 5 μL of the FITC-DMSO solution was added per ml hydrogel precursor; to stain alginate-gelatin with TRITC, 10 μL of the TRITC-DMSO solution per ml hydrogel precursor was added. The fluorescent working solutions were mixed into the hydrogel precursors at 40 °C with a spatula. Samples were printed and crosslinked equally to the cell-containing samples.

Samples from both groups were imaged alike in bottom view and lateral view with an inverted microscope (Olympus IX51, Volketswil, Switzerland) with a 2× objective. For the lateral view samples were sectioned into 1-mm thick slices. CellTracker™ Green as well as FITC stained hydrogel was visualized with the FITC filter (wavelength 530 nm, bandwidth 30 nm), CellTracker™ Red and TRITC stained hydrogel was detected with the TRITC filter (wavelength 590 nm, bandwidth 34 nm). Background noise of the images was removed and the image contrast was enhanced in the microscope software "cellSens Standard" by adapting the signal-to-light intensity range of the RGB channels in the histogram. Intensity of the images from the hydrogel-only group taken with the TRITC filter was reduced to a single intensity which varied between [139, 139] and [246, 246], depending on the image and its respective focus during imaging. The images from both channels were combined in the microscope software.

Generation of hollow channels

The direct generation of hollow channels within a hydrogel bulk is difficult due to the missing initial construct stability when bridging hollow structures with a hydrogel. A more elaborated approach is to fill channels during printing with a support material which is leached afterwards. Size of the printed channels, filled with gelatin, was varied between one, four and nine filaments, organized in matrices of 1, 2×2, and 3×3, like in Figure 1(D,G) and Figure 1(E,H). To strengthen the investigation of gelatin leaching depending on channel size, the channel composed of 3×3 filaments was additionally added. With a path width of 500 μm and a layer height of 350 μm, the expected sizes of the channels were 500×350 μm^2, 1000×700 μm^2, and 1500×1050 μm^2, respectively. The surrounding bulk material was constantly set to two layers of filaments in all directions for all constructs. In analogy to Influence of cell-embedding on feature size and shape section, alginate-gelatin hydrogel precursor was stained with FITC and gelatin was stained with TRITC before printing. Samples were printed and crosslinked as described in 3D bioprinting system section. A piece of 5 mm length was cut out of the 20 mm long samples with a razor blade from the middle of the samples for longitudinal imaging and a 1 mm thick disc for cross-sectional imaging. Samples were moved into eight-well nunc™ Lab-Tek™ Chambered Coverglass (Thermo Fisher Scientific, Wohlen, Switzerland)

filled with 500 μL PBS which additionally contained 0.25% (w/v) $CaCl_2$ to maintain the structural integrity of the constructs. Gelatin starts leaching once heated up above room temperature. The constructs were kept on ice until the first imaging time point was taken and moved to 37 °C to initialize gelatin leaching immediately after. Gelatin leaching was monitored with an inverted microscope and a 2× objective during 3 h with imaging time points after 30, 90, and 180 min to assess the formation of hollow channels. Before and after each imaging time point the well was carefully moved to generate medium fluctuation to distribute the leached gelatin in the well reducing the signal of the leached gelatin close to the object for imaging and to enhance gelatin leaching. The signal-to-light intensity ranges of the images were adjusted as described in Influence of cell-embedding on feature size and shape section.

Statistical analysis

All quantitative values are reported as means ± standard deviation with $n = 5$ samples per group. To compare groups, statistical analysis of variance (ANOVA) was performed using PASW Statistics 18 (SPSS, Chicago, IL), applying an univariate ANOVA with Bonferroni Post Hoc test. p values <0.05 were considered statistically significant and $p < 0.01$ highly statistically significant.

RESULTS

Printing channels in horizontal and vertical orientation

Filament-based 3D bioprinting requires at least two connected points in one printing layer to generate material output. To reduce a channel to the least possible amount of points based on that condition, the channel in vertical orientation was defined with four points in a 2 × 2 matrix. To be able to compare vertical- versus horizontal channel orientation, a horizontal channel consisting of four filaments, which corresponds to the four points in the vertical orientation, was added. It was observed during ink deposition that material accumulation occurred when printing curvatures. For straight channels in horizontal orientation curvatures were located only at the end of the construct and did not affect the area of interest [Fig. 1(A,B)]. In contrast, when printing straight channels in vertical orientation, where curvatures were present in the construct [Fig. 1(C)], material accumulation occurred in the middle of the geometry. This additional material deposition had to be compensated by providing enhanced lateral space. The distance between adjacent filaments had to be doubled for printing the vertical channels compared to the horizontal channels to be able to print a decent cylindrical geometry. Representative images of printed channels analyzed by μCT are illustrated in Figure 3 as negatives for a more informative presentation—implying that the channel phase is visible in the image instead of the hydroxyapatite-enhanced radiopaque bulk phase. The outer dimensions of the constructs are indicated with the box.

Channel cross-sectional area

Cross-sectional areas of the theoretical and the printed channels were evaluated; the parameters used for calculations are illustrated in Figure 2. For hydrogel precursor printing $d_{min,t} = 500$ μm was used for horizontal channels and $d_{min,t} = 1$ mm was used for vertical channels. Theoretical feature size for a horizontal channel consisting of a single filament was $s_{t,x} = 500$ μm and $s_{t,z} = 350$ μm considering a layer height of 350 μm, and for the horizontal channel consisting of four filaments it was $s_{t,x} = 1$ mm and $s_{t,z} = 700$ μm, respectively. For a vertical channel the calculation of the theoretical feature size led to $s_{t,x} = 2$ mm and $s_{t,y} = 2$ mm. Theoretical cross-sectional area of the hydrogel channels calculated with Eq. (1) was $A_t = 0.18$ mm^2 for a horizontal channel consisting of a single filament, $A_t = 0.7$ mm^2 for a horizontal channel consisting of four filaments and $A_t = 4$ mm^2 for a vertical channel (Table I).

The emulsion was printed with $d_{min,t} = 250$ μm for horizontal channels and $d_{min,t} = 500$ μm for vertical channels with a layer height of 250 μm; leading to $s_{t,x} = 250$ μm and $s_{t,z} = 250$ μm for a horizontal channel consisting of a single filament, $s_{t,x} = 500$ μm and $s_{t,z} = 500$ μm for a horizontal channel consisting of four filaments and $s_{t,x} = 1$ mm and $s_{t,y} = 1$ mm for a vertical channel, respectively. Theoretical cross-sectional area of the emulsion channels calculated with Eq. (1) was $A_t = 0.06$ mm^2 for a horizontal channel consisting of a single filament, $A_t = 0.25$ mm^2 for a horizontal channel consisting of four filaments and $A_t = 1$ mm^2 for a vertical channel (Table I).

The printed samples were analyzed with μCT analysis regarding channel volumes. The average area over a certain length was calculated with Eq. (2) (Table I). For the printed hydrogel samples, channel cross-sectional areas were $A_p = 0.3 \pm 0.1$ mm^2 for horizontal channels consisting of a single filament, $A_p = 1.0 \pm 0.2$ mm^2 for horizontal channels consisting of four filaments and $A_p = 6.8 \pm 0.9$ mm^2 for vertical channels. Channel cross-sectional areas of printed emulsion samples were $A_p = 0.1 \pm 0.0$ mm^2 for horizontal channels consisting of a single filament, $A_p = 0.2 \pm 0.0$ mm^2 for horizontal channels consisting of four filaments and $A_p = 0.9 \pm 0.3$ mm^2 for vertical channels.

To compare printed to theoretical cross-sectional area of the different channels, the ratios of A_p/A_t were calculated (Table I). For the hydrogel groups the average A_p was larger than A_t. A_p was only in the range of A_t in the group with horizontal channels consisting of a single filament. For the hydrogel channels no statistical difference was detected between A_p of horizontal channels consisting of a single filament compared to horizontal channels consisting of four filaments. Channel orientation had a statistically significant effect at $p < 0.01$ in A_p between the vertical channels compared to the horizontal channels. For channels printed with emulsion the average A_p was smaller than A_t. A_p was only in the range of A_t in the group with vertical channels. For the emulsion channels statistically significant differences of A_p were consistent with the hydrogel group, with a statistically significant difference at $p < 0.01$ between the vertical channels and the horizontal channels, respectively. Plots in Figure 4 illustrate A_p (column) and A_t (dashed line) of the hydrogel and emulsion channels in the various orientations.

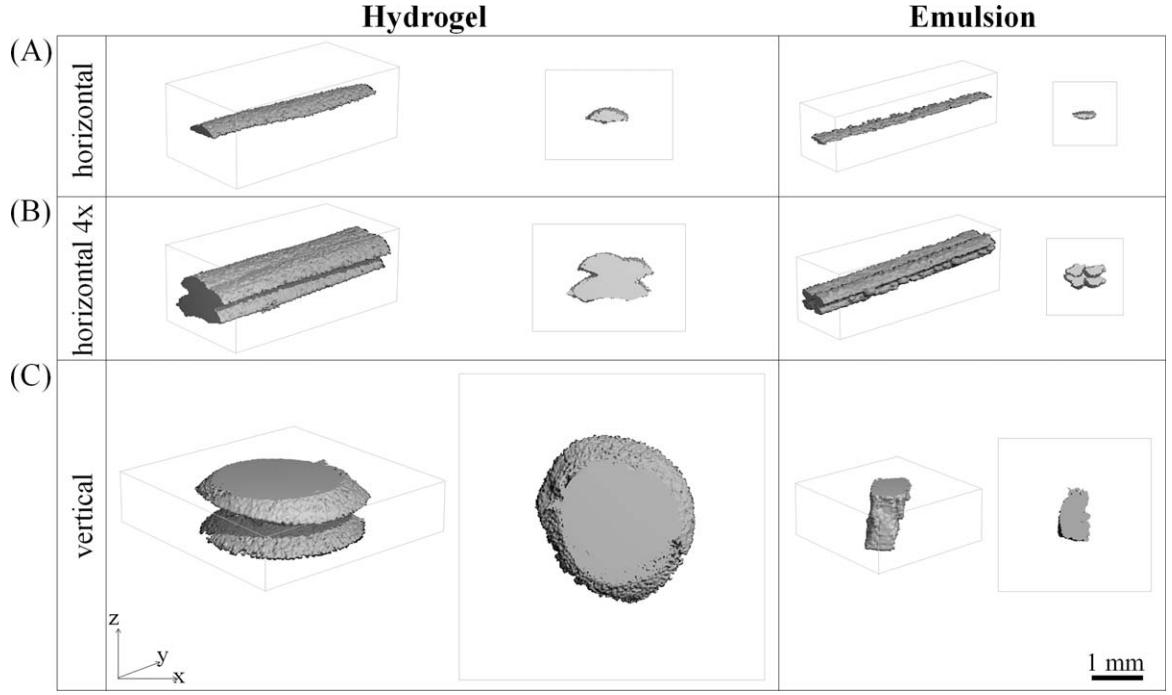

FIGURE 3. Negative images of printed channels in bulk material. The left column shows representative samples printed with hydrogel and the right column shows representative samples printed with emulsion. Row (A) shows the horizontal channels consisting of a single filament in bulk material, row (B) the horizontal channels consisting of four filaments in bulk material and row (C) the vertical channels in bulk material.

Structure orientation effects

To assess the influence of structure orientation on feature size, A_t and A_p were compared between the different channels and their deviation factors A_t/A_t and A_p/A_p summarized in Figure 5(A). A_t of the vertical hydrogel channel was 23× larger than A_t of the horizontal channel consisting of a single filament and 6× larger than A_t of the horizontal channel consisting of four filaments. For the emulsion, A_t was 16× and 4× larger, respectively. For printed hydrogel constructs, A_p of vertical channels was on average 23× larger compared to A_p of horizontal channels consisting of a single filament and on average 7× larger compared to A_p of horizontal channels consisting of four filaments. For printed emulsion constructs, A_p was on average 73× and 6× larger, respectively.

TABLE I. Theoretical Minimum Distance $d_{min,t}$, Theoretical Feature Size s_t, Theoretical Area A_t, Printed Area A_p and the Ratio of Printed to Theoretical Area A_t/A_p of Channels Printed With Hydrogel and the Emulsion for Horizontal and Vertical Channel Orientation with $n = 5$

Material	Orientation	$d_{min,t}$ (mm)	s_t (mm)	A_t (mm^2)	A_p (mm^2)
Hydrogel	Horizontal	0.5	0.5	0.18	0.3 ± 0.14
	Horizontal 4x	0.5	1	0.7	1.04 ± 0.2
	Vertical	1	2	4	6.81 ± 0.94
Emulsion	Horizontal	0.25	0.25	0.06	0.01 ± 0.01
	Horizontal 4x	0.25	0.5	0.25	0.15 ± 0.03
	Vertical	0.5	1	1	0.91 ± 0.28

Horizontal represents the horizontal channels consisting of a single filament, horizontal 4× the horizontal channels consisting of four filaments and vertical the channels in vertical orientation.

Regarding the influence on the shape, printed vertical channels revealed a more circular channel cross-section compared to the horizontal channels, which resulted in differently distinct flattened filaments (Fig. 3).

Material effects

To assess the influence of the ink on feature size, A_t and A_p were compared between the different materials used and A_t/A_t and A_p/A_p summarized in Figure 5(B). In theory, the cross-sectional area of the horizontal hydrogel channel consisting of a single filament is 3× larger compared to the horizontal emulsion channel consisting of a single filament. In reality, A_p of horizontal hydrogel channels consisting of a single filament was on average 24× larger compared to the corresponding emulsion channels. For horizontal hydrogel channels consisting of four filaments the areas were theoretically 3× larger and practically 7× larger on average compared to the corresponding emulsion channels. For the vertical channels, the area of the hydrogel channel is theoretically 4× larger than the area of the emulsion channel and resulted in an average of a 7× larger area of printed hydrogel channels compared to emulsion channels.

Regarding the influence on the shape, individual filaments of the hydrogel did not keep the round shape and flattened—leading to the path width of 500 μm and layer height of 350 μm. Adjacent filaments merged and one connected channel was achieved. Single filaments of the emulsion were structurally more stable and the round shape of the initial filament flattened only slightly during deposition. Adjacent filaments of the emulsion did not fully merge [Fig. 3(B)]. Hydrogel channels in vertical orientation revealed a

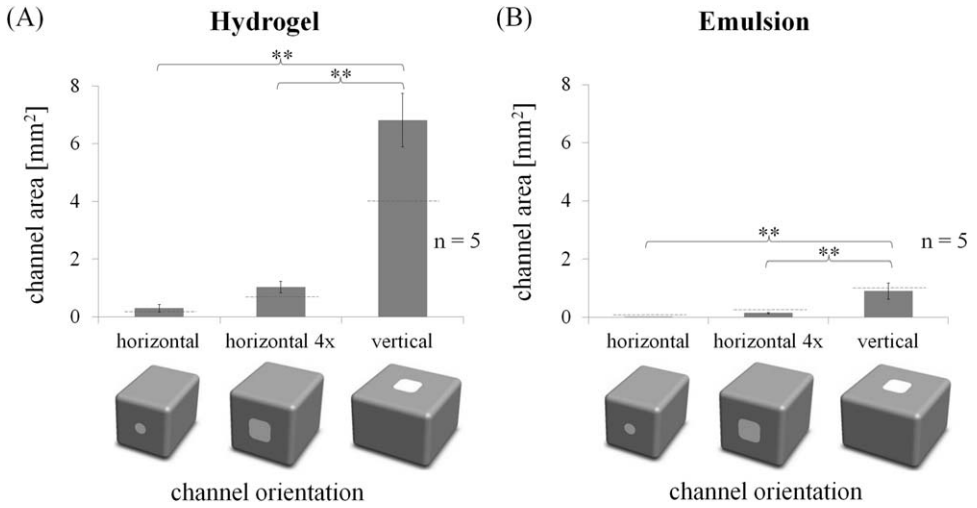

FIGURE 4. Theoretical (A_t) and printed (A_p) channel cross-sectional area of (A) the hydrogel and (B) the emulsion. A_t is illustrated with a dashed line; A_p is illustrated as column and indicated as means ± standard deviation with $n = 5$. *$p < 0.05$, **$p < 0.01$. The values correspond to A_t and A_p from Table I.

circular channel cross-section but an inhomogeneous channel shape with visible influences from the printing layers, while the cross-section of emulsion channels in vertical orientation was rather square but a homogeneous channel shape in the longitudinal axis was achieved. The connection between adjacent hydrogel filaments was strengthened with the chemical crosslinking after printing and the printed structure was much stronger compared to the emulsion.

More complex channel geometries

More complex channel geometries in the shape of L, T, S, U, and X were printed within bulk material. Schematics of the printing paths which were used to generate the different channels and the bulk phase are illustrated in Figure 6(A). Qualitative analysis performed by μCT [Fig. 6(B)] showed the feasibility of printing the different geometries consisting of various rectangular elements and intersections with connecting channels. Material accumulation in the channel structures was visible at curvatures. For sequential rectangular elements near each other, such as at the S-shape, the material accumulation was even further enhanced and had to be compensated with a locally larger feature size for printing; in contrast to multiple rectangular elements with larger distance, such as the U-shape. The additional material got dragged into the curvature of rectangular elements nearby. Additionally, a difference in layer height was noticed at the intersection of connecting channels for all samples. The ratios between printed channel volumes quantitatively analyzed with μCT and theoretical channel volumes were between 1.3 and 2.4 (Table II), implying that the printed channels all had larger volumes compared to the theoretical channels.

Influence of cell-embedding on feature size and shape

To assess the influence of cell-embedding, fluorescently labeled cells with a different color for each phase were embedded into the hydrogel and compared to an equal setup without cells in which the two hydrogel phases were fluorescently stained. The geometries used in More complex channel geometries section could be printed with cell-containing bioink with the same feature size as the pure hydrogel and allowed channel fabrication in equal size [Fig.

(A) Structure orientation effect

		vertical			
		A_t / A_t [1]		A_p / A_p [1]	
		hydrogel	emulsion	hydrogel	emulsion
horizontal	horizontal	23	16	23	73
	horizontal 4x	6	4	7	6

(B) Material effect

		hydrogel	
		A_t / A_t [1]	A_p / A_p [1]
emulsion	horizontal	2,8	24
	horizontal 4x	2,8	7
	vertical	4	7

FIGURE 5. Structure orientation effects (A) and material effects (B) on theoretical and printed channels made of hydrogel or emulsion in horizontal and vertical orientation. Effects are indicated with deviation factors A_t/A_t and A_p/A_p. For example was A_t of the hydrogel channel in vertical orientation 23× larger than A_t of the hydrogel channel consisting of a single filament in horizontal orientation. Horizontal represents horizontally oriented channels consisting of a single filament, horizontal 4× horizontally oriented channels consisting of four filaments and vertical channels in vertical orientation.

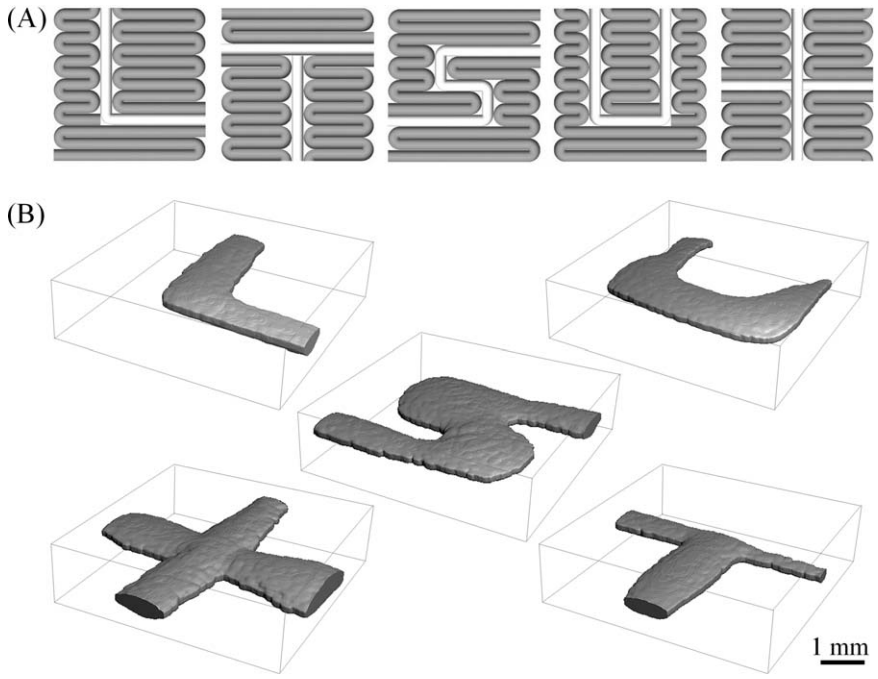

FIGURE 6. (A) schematics of different channel geometries embedded in the bulk material. (B) negative μCT images of the 3D printed hydrogel constructs. The outer dimensions of the investigated volume of interest are indicated with the box.

7(A,B)]. Comparing the representative images of the cell-containing group to the hydrogel-only group [Fig. 7(A–D)], the shape of curvatures and intersections were more imprecise for the cell-containing structures compared to the non-cellular structures, whereas no difference in the shape of the straight parts of the structures was detected. Cells were homogeneously distributed in the material and stayed within their phase after printing and crosslinking.

Generation of hollow channels

The creation of hollow channels within a bulk-material consisting of alginate-gelatin hydrogel was achieved by using gelatin as support material for the channel phase during printing and leaching the gelatin subsequently once the construct was printed. Figure 8 illustrates schematics of the investigated geometries as well as fluorescent images of the printed samples in longitudinal and cross-sectional view. The representative fluorescent images indicate the leaching of gelatin during 3 h at 37 °C, with the amount of remaining gelatin correlating with the orange TRITC signal. Gelatin leaching took place continuously in all samples starting at the interface between channel and bulk material. After 3 h only a weak TRITC signal was detected in all groups, indicating that the support material was almost completely leached from the smallest to the largest channel size. The bulk material remained stable revealing an intact hollow channel after gelatin leaching.

TABLE II. Volume Analysis of the More Complex Channel Structures Printed With Hydrogel ($n = 1$)

Geometry	V_p (mm^3)	V_t (mm^3)	V_p/V_t (L)
L-shape	1.7	1.3	1.3
T-shape	2.2	1.6	1.3
S-shape	4.1	2.1	1.9
U-shape	2.9	1.7	1.7
X-shape	4.6	1.9	2.4

Channel volume of printed geometries V_p, theoretical channel volume V_t within the same VOI, and the ratio of printed to theoretical channel volume V_p/V_t are compared.

DISCUSSION

The 3D bioprinting promises high potential for the fabrication of more complex filled or hollow stable channels which cannot be generated with conventional methods. To improve channel fabrication with filament-based deposition, the main interests of this study were to determine the influence of structure orientation and ink on the smallest possible feature size and shape of the channels, the influence of the printed geometry and embedded cells. The findings show that these influences significantly affect the resulting channels, and will serve as basis for the design of larger constructs containing channels for filament-based deposition. More sophisticated 3D channels filled with a stimulative environment will help to overcome certain limitations in nerve regeneration[5] or to generate hollow channels for tissue engineering larger constructs to improve nutrients and oxygen supply.

As expected, structure orientation did have a remarkable influence on filament-based printed objects. We assumed that the minimum of two points in one plane needed to induce the material outflow is the main cause for larger vertically aligned structures, since these points were orthogonal to the channel axis—in contrast to horizontal structures where the two points were on the channel axis and the

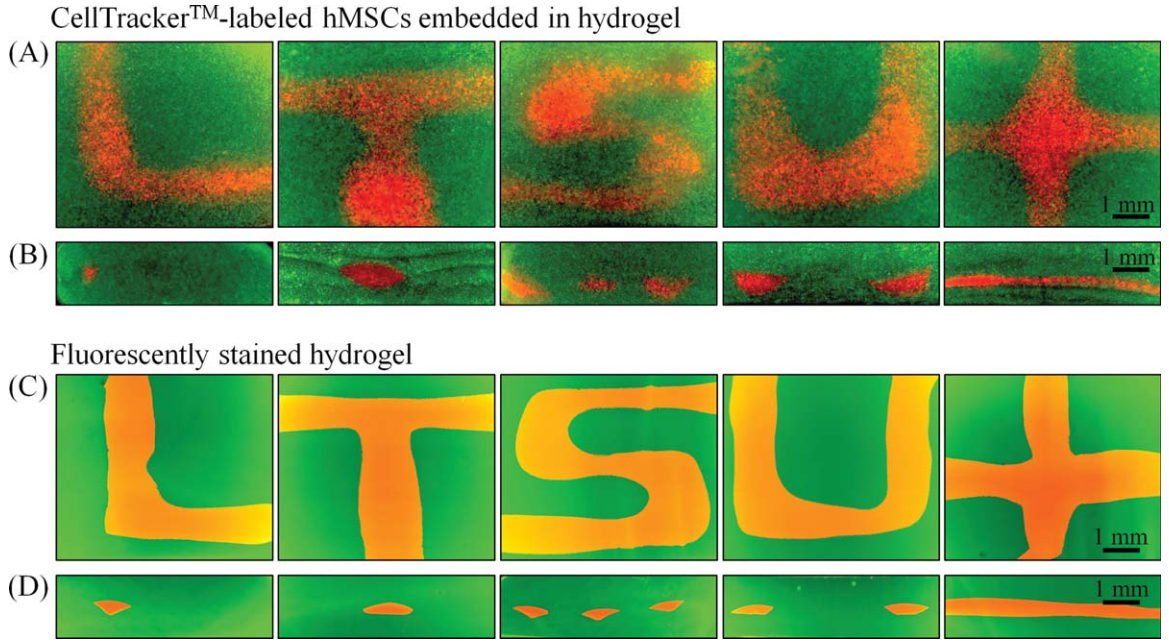

FIGURE 7. Fluorescent images of hydrogel constructs with different channel geometries. (A) and (B) show printed CellTracker™-labeled hMSCs embedded in the bulk phase (green) and in the channel phase (red). (C) and (D) show hydrogel samples without cells stained with FITC in the bulk phase (green) and TRITC in the channel phase (orange). Images in (A) and (C) are illustrated in bottom view, images in (B) and (D) in lateral view. [Color figure can be viewed in the online issue, which is available at wileyonlinelibrary.com.]

most simple channel structure consisted of only one filament [Figs. 1(A,C) and 2]. Surprisingly, the results revealed an equally significant influence due to additional material deposition in vertical channels. Material accumulation took place at curvatures and the additional material had to be compensated by extending the minimum distance between adjacent filaments when curvatures were located in the middle of the geometry, which was the case for vertical channels [Fig. 1(F)]. For horizontal channels printed with straight filaments the additional material was eluded at the open border and did not affect the structure of the channels [Fig. 1(D–E)]. Both applied inks, hydrogel, and emulsion, were affected equally. It seems that most 3D printed constructs are affected from material accumulation at

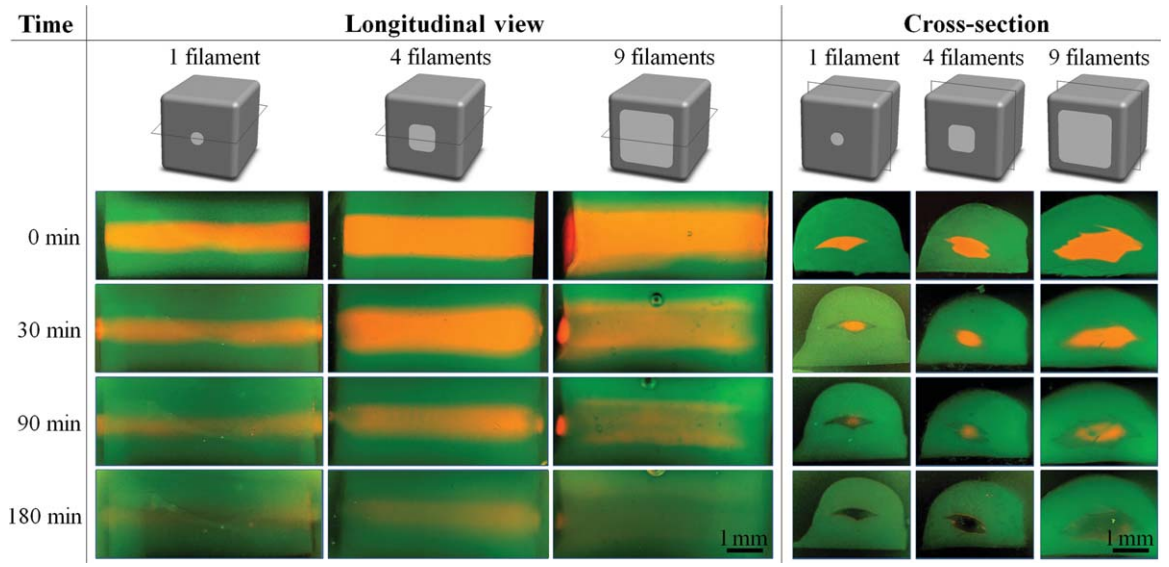

FIGURE 8. Gelatin leaching to generate hollow channels embedded in a hydrogel bulk. Schematics of the constructs indicate the different sizes of the hollow channels and the image orientation. Representative fluorescent images of the samples in longitudinal and cross-sectional view are illustrated at different time points (0, 30, 90, and 180 min). Bulk phase (green) contains alginate-gelatin hydrogel and is labeled with FITC; channel phase (orange) contains gelatin and is labeled with TRITC. The intensity of the orange dye indicates the remaining gelatin. [Color figure can be viewed in the online issue, which is available at wileyonlinelibrary.com.]

curvatures, for example the printed agar[30] or hydroxyapatite scaffold.[31,32] However in the majority of the studies the geometry itself is not affected since it is printed with straight filaments[20–22] and the additional material can be eluded at the open border. Material accumulation is not always equally distinctive and is sometimes less visible, such as the curved hydrogel channel in Ref. 25 which is embedded in a hydrogel bulk with the same color. Material accumulation could probably be reduced by a locally faster printing speed or lower deposition rate at curvatures. The option to change one of these two parameters during the fabrication of a construct, however, was not provided by Fab@Home. Differences in filament shape of the different inks are clearly visible in Figure 3. We assume that the shape of a filament is related to material characteristics such as viscosity, rheological behavior and surface tension but also to the printing- and solidification process. One previous study assigned the effect of different fiber diameters and scaffold architectures of various hydrogels to their gelation rate,[33] another study reported the influence of the ink on path width and length.[26] Path width and layer height reflected the shape of the filament cross-section, with a width-to-height ratio of 1:1 for round filaments such as the emulsion and a larger width-to-height ratio for oval cross-sections as it was the case for the hydrogel used in this study. The larger width-to-height ratio of deposited filaments is often found in hydrogel printing. For example PEG-DA used in Ref. 26 was printed with 800 μm path width and 600 μm layer height and pure alginate was implemented with 800 μm path width and 190 μm layer height.[23] However, the shape of a printed filament is not related to the mechanical stability of the whole construct. The emulsion filament almost kept its shape as it was deposited from the printer without crosslinking procedure, but the printed construct completely lacked mechanical stability; it collapsed at the slightest contact. The hydrogel in contrast flattened during deposition but revealed strong mechanical integrity after crosslinking.

The used ink had a significant influence on the smallest possible distance between adjacent filaments and thus the feature size to print a decent geometry (Table I). In case the value of the theoretical area was within the range of the associated areas from printed channels the printing parameters were properly chosen (Fig. 4). This was only achieved for one group per ink. To define printing parameters which exactly fit geometries in different orientations is challenging. The A_p/A_t ratios indicate whether the theoretical area is underestimated ($A_p/A_t > 1$), or overestimated ($A_p/A_t < 1$). The overestimated area is also visible as cavities within the printed object, which can be seen in the emulsion channel in horizontal orientation consisting of four filaments in Figure 3(B).

Other groups using bioinks with comparable properties to the hydrogel used in this study reached similar or even larger minimal feature sizes with a filament-based deposition; they printed alginate-gelatin with 800 μm path width,[14] alginate with 800 μm,[23] hyaluronan with 500 μm[34] or PEG-DA with 800 μm.[26] Smaller feature sizes were achieved by printing pure gelatin (7% (w/v)) with a path width of 400 μm[24] or pure alginate (2 mg mL^{-1}) with 300 μm.[33] Both inks were less viscous compared to the bioink containing 10% (w/v) gelatin plus 2% (w/v) alginate in this study, which probably allowed printing smaller features. The gelatin concentration in Ref. 24 was sufficient for its application as temporary support material; the pure alginate printed in a $CaCl_2$-bath to generate 3D constructs resulted in a limited stacking of multiple layers.[33] We observed in a previous study that alginate printed directly in a $CaCl_2$-bath cannot bind between layers.[15] In our hydrogel, gelatin induced immediate construct stability allowing for the alginate to be crosslinked only after fabrication, which enabled binding between layers and the generation of a mechanical integer 3D construct. The inclusion of hydroxyapatite enabled visualization of the printed construct with μCT. This favorable combination was a compromise which resulted in a slightly larger minimal feature size. With a lower resolution an overall larger size of the 3D construct can be achieved, as printing resolution is directly related to the size of the biofabricated sample.[8] Time is restricted if living cells are included in the printing process: A lengthy exposure of cells to the high stress level during processing can be detrimental, and hydrogels desiccate over time.

A higher printing resolution and greater scaffold stability can be achieved with different methods. For printing scaffold material only, a larger variety of materials, crosslinking and/or post-treatment procedures can be applied since potential cytotoxic substances can be removed after scaffold fabrication, would allow for an ink with more favorable printing characteristics.[35] In that case cells can be seeded afterwards; however, this excludes the advantage of a targeted cell placement within the 3D construct given by the cell-based 3D bioprinting. Smaller feature sizes could also be achieved for example with inkjet printing, which was used to print fibrin fibers containing endothelial cells with 93 μm fiber diameter.[21] During inkjet printing cells are exposed to higher shear forces induced by the small fluid volumes which may cause damage to cells.[36] Inkjet printing requires less viscous substrate solutions and the final constructs result in an overall smaller size due to limited construct stability especially in 3D—examples using inkjet printing in combination with hydrogels are therefore rather limited.[35] With the focus on a combined cell-biomaterial deposition to generate 3D tissues, more requirements on the bioink and the printing process have to be fulfilled, which implies the compromise in resolution. However there is large potential to further develop this approach, especially from the materials technology side. The associated crosslinking process to achieve stable constructs has to be considered since it strongly affects gelation time and resulting strength of the hydrogel, may induce clogging of the printing tip during fabrication and often entails unwanted cytotoxic side-products. Printed agarose filaments, for example, fused under their own weight due to the slow gelation rate.[33] A chitosan scaffold crosslinked with sodium hydroxide- ethanol was biocompatible when seeded with cells afterwards[37]; however, the crosslinker is detrimental to cells and cannot be used for cell-

embedding. Also 2-photon-polymerization, which allowed PEG-DA scaffold fabrication in nm resolution, is not suitable for cell embedding since residual material from the used photoinitiators seemed to diffuse out of the polymer and resulted in impaired cell viability.[38]

The geometry did have an influence on feature size and shape of the printed channels, which is no surprise regarding the findings about material accumulation at curvatures in the middle of an object. Additional material which was deposited at sequential rectangular elements in short distance to each other such as the S-shape had to be compensated with a locally larger path width in the printing script resulting in a locally larger feature size in the final construct. However, this did not affect the ratios of printed to theoretical channel volumes in the VOI of the complex channels, which were within the range of hydrogel channels consisting of a single filament in horizontal orientation (Tables I and II). Anyhow, a trend toward a higher ratio of printed to theoretical channel volume was detected of geometries with more rectangular elements and intersections such as the S- and X-shape, which coincides with the observations from the qualitative image analysis regarding material accumulation and shape deformation. For the investigation of more complex channels a horizontal orientation was chosen due to the smaller possible feature sizes; nerve regeneration was for example addressed in the range between 100 and 600 μm.[7] The smaller branched channels could be connected, if needed, with larger channels in vertical orientation.

The embedding of cells in the bioink is a great advantage of 3D biofabrication allowing the generation of elaborated cell-based 3D tissue constructs. Multiple cell types can be printed in specific locations overcoming limitations of random cell distribution and uncontrolled ingrowth due to cell seeding by hand.[39] However, the addition of cells to the hydrogel precursor altered the concentration of the bioink—and as we showed, the ink can significantly affect the printed filaments and thus the shape of the 3D construct (Material effects section). The more complex channel structures were used to compare printed hydrogel channels with [Fig. 7(A,B)] and without cells [Fig. 7(C,D)] to assess various facets of printing with multiple straight and rectangular elements as well as crossings. Embedding of cells did not influence material behavior during printing and led to the same feature size as obtained for hydrogel-only samples. The slightly less precise shape of the cell-containing hydrogel channels and a slightly weaker construct can be related to the reduced hydrogel concentration, which might have resulted in less spots for the crosslinker to attach. As it has been shown, cellular self-assembly is a powerful mechanism of engineering tissue, as the example of a self-assembled branched structure built of fibroblast spheroids has shown.[11] Therefore, the slightly changed ink properties are not expected to have a negative influence on tissue engineering. Printing channels containing living cells shows great potential for tissue reconstruction especially when cells in adjacent phases stay in their location but the phases remain physically connected after crosslinking, which was the case in this study.

Hollow channels could for example be important for nutrient and oxygen transport as well as the removal of waste products. The successful generation of hollow channels requires a setup which allows the removal of the support structure in the channel phase as well as a stable 3D bulk construct during and after processing. Gelatin was almost completely leached within only 3 h for all printed channels independent of their size (Fig. 8). From the cross-sectional images it could be observed that gelatin leaching started at the interface of the support structure, with the gelatin in the middle of the support phase being only leached after 3 h. The generation of channels in an alginate-gelatin bulk material with gelatin as support structure showed advantages compared to other approaches. The smallest hollow channel generated via alginate leaching in gelatin methacrylamide-gellan hydrogel had a diameter of 4 mm,[23] compared to the smallest hollow channel of $500 \times 350\ \mu m^2$ presented herein. Smaller vessels with 300 μm in diameter were achieved with scaffold-free cell printing,[11] but the lack of mechanical integrity, which is usually provided by the hydrogel, limits this technique to small constructs.

In this study the generation of filled and hollow channels within 3D constructs made by filament-based 3D bioprinting was investigated using the smallest possible feature size for every setup. Parameters examined included those potentially influencing feature size and shape of the channels, in particular structure orientation, ink, geometry, and cell-embedding.

CONCLUSION

A systematic investigation revealed a significant influence of structure orientation, geometry and ink on the smallest possible feature size and shape of filament-based printed 3D channels. The influence on feature size could mainly be attributed to the need of connecting two points in one printing plane in filament printing and to material accumulation at curvatures of the printing path which affected vertically oriented channels. Material accumulation occurred also at more complex geometries with multiple rectangular elements nearby or crossings and is therefore important to consider when designing tissue constructs and the corresponding printing path. On the basis of these results we suggest designing complex channels with rectangular elements with minimum three path width distance to limit the increase in feature size by avoiding excessive material accumulation. Because of the significant influence of the ink on feature size and shape of the channels the material should be analyzed prior to 3D tissue printing. Adding cells to the hydrogel did not alter feature size and shape of the channels. Hollow channels could be generated in different sizes within the same time. For alginate-gelatin (-hydroxyapatite), the smallest printed channel was $500 \times 350\ \mu m^2$ for filled channels as well as for hollow channels using gelatin as support material. The 3D constructs with anisotropic structures could be organized to produce the best possible outcome. For the design of larger constructs with a branched channel-system it would imply larger channels orientated vertically and smaller branched channels oriented horizontally. The cell-hydrogel system presented in this study provides a solid basis for the generation of filled and hollow

3D channels for various tissues with the potential to be further developed to address applications such as nerve generation or vasculature.

ACKNOWLEDGMENTS

The authors acknowledge Marie E. Godla, Michael Vogt, and Vitaly Koren from the Institute for Biomechanics, ETH Zurich for preliminary experiments.

REFERENCES

1. Khademhosseini A, Vacanti JP, Langer R. Progress in tissue engineering. Sci Am 2009;300:64–71.
2. Bian L, Angione SL, Ng KW, Lima EG, Williams DY, Mao DQ, Ateshian GA, Hung CT. Influence of decreasing nutrient path length on the development of engineered cartilage. Osteoarthritis Cartilage 2009;17:677–685.
3. Huang G, Wang S, He X, Zhang X, Lu TJ, Xu F. Helical spring template fabrication of cell-laden microfluidic hydrogels for tissue engineering. Biotechnol Bioeng 2013;110:980–989.
4. Thuret S, Moon LDF, Gage FH. Therapeutic interventions after spinal cord injury. Nat Rev Neurosci 2006;7:628–643.
5. Steed MB, Mukhatyar V, Valmikinathan C, Bellamkonda RV. Advances in bioengineered conduits for peripheral nerve regeneration. Atlas Oral Maxillofac Surg Clin 2011;19:119–130.
6. Zhu N, Li MG, Guan YJ, Schreyer DJ, Chen XB. Effects of laminin blended with chitosan on axon guidance on patterned substrates. Biofabrication 2010;2:045002
7. Wang A, Ao Q, Cao W, Yu M, He Q, Kong L, Zhang L, Gong Y, Zhang X. Porous chitosan tubular scaffolds with knitted outer wall and controllable inner structure for nerve tissue engineering. J Biomed Mater Res A 2006;79A:36–46.
8. Wüst S, Müller R, Hofmann S. Controlled positioning of cells in biomaterials—Approaches towards 3D tissue printing. J Funct Biomater 2011;2:119–154.
9. Fedorovich NE, Alblas J, de Wijn JR, Hennink WE, Verbout AJ, Dhert WJ. Hydrogels as extracellular matrices for skeletal tissue engineering: State-of-the-art and novel application in organ printing. Tissue Eng 2007;13:1905–1925.
10. Mironov V, Trusk T, Kasyanov V, Little S, Swaja R, Markwald R. Biofabrication: a 21st century manufacturing paradigm. Biofabrication 2009;1:022001
11. Norotte C, Marga FS, Niklason LE, Forgacs G. Scaffold-free vascular tissue engineering using bioprinting. Biomaterials 2009;30:5910–5917.
12. Derby B. Printing and prototyping of tissues and scaffolds. Science 2012;338:921–926.
13. Balakrishnan B, Jayakrishnan A. Self-cross-linking biopolymers as injectable in situ forming biodegradable scaffolds. Biomaterials 2005;26:3941–3951.
14. Duan B, Hockaday LA, Kang KH, Butcher JT. 3D bioprinting of heterogeneous aortic valve conduits with alginate/gelatin hydrogels. J Biomed Mater Res A 2013; 101:1255–1264. **A**
15. Wüst S, Godla ME, Müller R, Hofmann S. Tunable hydrogel composite with two-step processing in combination with innovative hardware upgrade for cell-based three-dimensional bioprinting. Acta Biomater 2014;10:630–640.
16. Barradas AM, Yuan H, van Blitterswijk CA, Habibovic P. Osteoinductive biomaterials: Current knowledge of properties, experimental models and biological mechanisms. Eur Cell Mater 2011;21:407–429.
17. Bohner M, van Lenthe GH, Grünenfelder S, Hirsiger W, Evison R, Müller R. Synthesis and characterization of porous [beta]-tricalcium phosphate blocks. Biomaterials 2005;26:6099–6105.
18. Lin H-R, Yeh Y-J. Porous alginate/hydroxyapatite composite scaffolds for bone tissue engineering: Preparation, characterization, and in vitro studies. J Biomed Mater Res B Appl Biomater 2004;71B:52–65.
19. Zimmermann H, Shirley S, Zimmermann U. Alginate-based encapsulation of cells: Past, present, and future. Curr Diabet Rep 2007;7:314–320.
20. Li S, Xiong Z, Wang X, Yan Y, Liu H, Zhang R. Direct fabrication of a hybrid cell/hydrogel construct by a Double-nozzle assembling Technology. J Bioactive Comp Polym 2009;24:249–265.
21. Cui X, Boland T. Human microvasculature fabrication using thermal inkjet printing technology. Biomaterials 2009;30:6221–7.
22. Skardal A, Zhang J, McCoard L, Xu X, Oottamasathien S, Prestwich GD. Photocrosslinkable hyaluronan-gelatin hydrogels for Two-step bioprinting. Tissue Eng A 2010;16:2675–2685.
23. Visser J, Peters B, Burger TJ, Boomstra J, Dhert WJA, Melchels FPW, Malda J. Biofabrication of multi-material anatomically shaped tissue constructs. Biofabrication 2013;5:035007.
24. Lee W, Lee V, Polio S, Keegan P, Lee J-H, Fischer K, Park J-K, Yoo S-S. On-demand three-dimensional freeform fabrication of multilayered hydrogel scaffold with fluidic channels. Biotechnol Bioeng 2010;105:1178–1186.
25. Zhang Y, Yu Y, Chen H, Ozbolat IT. Characterization of printable cellular micro-fluidic channels for tissue engineering. Biofabrication 2013;5:025004.
26. Kang KH, Hockaday LA, Butcher JT. Quantitative optimization of solid freeform deposition of aqueous hydrogels. Biofabrication 2013;5:035001.
27. Hildebr T, Laib A, Müller R, Dequeker J, Rüegsegger P. Direct three-dimensional morphometric analysis of human cancellous bone: Microstructural data from spine, femur, iliac crest, and calcaneus. J Bone Miner Res 1999;14:1167–1174.
28. Stauber M, Müller R. Micro-computed tomography: A method for the non-destructive evaluation of the three-dimensional structure of biological specimens. Methods Mol Biol 2008;455:273–292.
29. Hofmann S, Hagenmüller H, Koch AM, Müller R, Vunjak-Novakovic G, Kaplan DL, Merkle HP, Meinel L. Control of in vitro tissue-engineered bone-like structures using human mesenchymal stem cells and porous silk scaffolds. Biomaterials 2007;28:1152–1162.
30. Landers R, Hübner U, Schmelzeisen R, Mülhaupt R. Rapid prototyping of scaffolds derived from thermoreversible hydrogels and tailored for applications in tissue engineering. Biomaterials, 2002;23:4437–4447.
31. Carvalho C, Landers R, Mulhaupt R, Hubner U, Schmelzeisen R. Fabrication of soft and hard biocompatible scaffolds using 3D-Bioplotting™. In 2nd, International Conference on Advanced Research and Rapid Prototyping; Virtual Modeling and Rapid Manufacturing. Leiria, Portugal: Taylor and Francis; 2005.
32. Bartolo PJS, Almeida H, Laoui T. Rapid prototyping and manufacturing for tissue engineering scaffolds. Int J Comput Appl Technol 2009;36:1–9.
33. Fedorovich NE, De Wijn JR, Verbout AJ, Alblas J, Dhert WJ. Three-dimensional fiber deposition of cell-laden, viable, patterned constructs for bone tissue printing. Tissue Eng A 2008;14:127–133.
34. Skardal A, Zhang J, Prestwich GD. Bioprinting vessel-like constructs using hyaluronan hydrogels crosslinked with tetrahedral polyethylene glycol tetracrylates. Biomaterials 2010;31:6173–6181.
35. Billiet T, Vandenhaute M, Schelfhout J, Van Vlierberghe S, Dubruel P. A review of trends and limitations in hydrogel-rapid prototyping for tissue engineering. Biomaterials 2012;33:6020–6041.
36. Ringeisen BR, Othon CM, Barron JA, Young D, Spargo BJ. Jet-based methods to print living cells. Biotechnol J 2006;1:930–948.
37. Ang TH, Sultana FSA, Hutmacher DW, Wong YS, Fuh JYH, Mo XM, Loh HT, Burdet E, Teoh SH. Fabrication of 3D chitosan-hydroxyapatite scaffolds using a robotic dispensing system. Mater Sci Eng C 2002;20:35–42.
38. Ovsianikov A, Malinauskas M, Schlie S, Chichkov B, Gittard S, Narayan R, Löbler M, Sternberg K, Schmitz KP, Haverich A. Three-dimensional laser micro- and nano-structuring of acrylated poly(ethylene glycol) materials and evaluation of their cytoxicity for tissue engineering applications. Acta Biomater 2011;7:967–974.
39. Thimm BW, Wüst S, Hofmann S, Hagenmüller H, Müller R. Initial cell pre-cultivation can maximize ECM mineralization by human mesenchymal stem cells on silk fibroin scaffolds. Acta Biomater 2011;7:2218–2228.